J. Fluid Mech. (2011), *vol.* 681, *pp.* 24–47.
doi:10.1017/jfm.2011.223

A two-dimensional model of low-Reynolds number swimming beneath a free surface

DARREN CROWDY[1]†, SUNGYON LEE[2], OPHIR SAMSON[1], ERIC LAUGA[3] AND A. E. HOSOI[2]

[1]Department of Mathematics, Imperial College, London SW7 2AZ, UK

[2]Hatsopoulos Microfluids Laboratory, Department of Mechanical Engineering, Massachusetts Institute of Technology, 77 Massachusetts Avenue, Cambridge, MA 02139, USA

[3]Department of Mechanical and Aerospace Engineering, University of California San Diego, 9500 Gilman Drive, La Jolla CA 92093-0411, USA

(Received 17 March 2010; revised 25 April 2011; accepted 11 May 2011; first published online 29 June 2011)

Biological organisms swimming at low-Reynolds number are often influenced by the presence of rigid boundaries and soft interfaces. In this paper, we present an analysis of locomotion near a free surface with surface tension. Using a simplified two-dimensional singularity model and combining a complex variable approach with conformal mapping techniques, we demonstrate that the deformation of a free surface can be harnessed to produce steady locomotion parallel to the interface. The crucial physical ingredient lies in the nonlinear hydrodynamic coupling between the disturbance flow created by the swimmer and the free boundary problem at the fluid surface.

Key words: interfacial flows (free surface), low-dimensional models, low-Reynolds number flows

1. Introduction

Low-Reynolds number swimming near solid boundaries or interfaces can exhibit interesting and unexpected features. In particular, the presence of long-range interactions typical of flows at low-Reynolds numbers implies that, in general, boundary effects can not be ignored (Brennen & Winet 1977; Lauga & Powers 2009). For instance, *E. coli* cells are observed to change their swimming trajectories from straight to circular when they are moving parallel to a solid surface (Maeda *et al.* 1976; Berg & Turner 1990; Frymier & Ford 1997; Lauga *et al.* 2006), a behaviour modification which may have important implications in the formation of biofilms (Costerton *et al.* 1995). The motion of micro-organisms near soft interfaces, such as spermatozoa motility through the mucus-filled female reproductive track (Suarez & Pacey 2006), is even more intriguing as the nonlinear coupling between the motion of the swimmer and the changing shape of the interfaces adds an extra level of complexity to the problem. Urzay (2010) has recently looked at the force-driven motion of low-Reynolds number particles in the lubrication limit and has addressed the coupling between the flow and the surface deformation.

The study of low-Reynolds number swimmers near a no-slip wall has received considerable attention in the past, and we refer to the reviews by Brennen &

† Email address for correspondence: d.crowdy@imperial.ac.uk

Winet (1977) and Lauga & Powers (2009) for a discussion of the relevant literature. Most theoretical work has focused on quantifying the change in swimming speed and energetics near solid boundaries (Reynolds 1965; Katz 1974; Katz, Blake & Paverifontana 1975; Katz & Blake 1975; Fauci & Mcdonald 1995). More recent work has addressed the dynamics of confined swimmers and tackled the subtle interplay between the time evolution of a swimmer's orientation and its position. For example, a well-known feature of swimming near a solid boundary is that organisms moving at low-Reynolds number tend to be attracted to solid surfaces (Rothschild 1963; Winet, Bernstein & Head 1984; Fauci & Mcdonald 1995; Cosson, Huitorel & Gagnon 2003; Woolley 2003; Hernandez-Ortiz, Stoltz & Graham 2005; Berke *et al.* 2008). This phenomenon can be rationalized by a fundamentally hydrodynamical mechanism in which the interaction with the rigid boundary causes a swimmer to reorient itself in such a way that it is eventually attracted to its hydrodynamic image system in the wall (Berke *et al.* 2008).

Other studies have revealed additional dynamical features of a swimmer's behaviour near a wall. Or & Murray (2009) have conducted numerical experiments to understand the wall-bounded dynamics of model swimmers from a control and dynamical systems perspective. In addition to the existence of a steady state in which the swimmers travel in a steady rectilinear motion parallel to the wall, the authors found that the generic motion of a swimmer can be described by nonlinear periodic orbits along the wall with complicated spatio-temporal structure. These observations have since been corroborated by laboratory experiments involving small robotic swimmers in a tank of viscous fluid (Zhang, Or & Murray 2010). Motivated by these studies, Crowdy & Or (2010) have recently proposed a simple two-dimensional model of a swimmer near a wall. Using a complex variable formulation of the problem, they obtained results in agreement with those of Or & Murray (2009) and Zhang *et al.* (2010). Crowdy (2011) has recently provided additional analysis to confirm that the dynamics of the point singularity description of Crowdy & Or (2010) is in excellent qualitative agreement with the unapproximated dynamics. This lends support for the use of simple point singularity swimmer models.

In the current paper, we address the coupling between a low-Reynolds number swimmer and a surface which can deform and focus on the case of a free interface with surface tension. Previous work considered how the unsteady deformation of soft surfaces generated by time-reversible flows could provide new modes of locomotion and pumping (Trouilloud *et al.* 2008). Here we ask the following question: Can a low-Reynolds number body exploit the deformation of a free surface to swim steadily?

Our study was originally motivated by the discovery of a peculiar mode of locomotion employed by water snails that crawl underneath the free surface. Separated from the interface by a thin layer of mucus, these organisms deform their foot to create a lubrication flow inside the mucus layer. This flow results in deformations of the free surface, which in turn rectifies the flow, allowing the water snails to move (Lee *et al.* 2008). The analysis in this paper contained two significant constraints, namely the gap between the swimmer and the air–water interface was assumed to be thin, and the deformation of the free surface was assumed to be asymptotically small. The work in the current paper removes these constraints and considers a more general mechanism for a swimmer translating steadily beneath the free surface.

Low-Reynolds number swimmers exert no net force and no net torque on the flow, and it is precisely these constraints that dictate the subsequent speed of the swimmer and its angular velocity. Here we introduce a mathematical representation of the swimmer as a two-dimensional torque-free point stresslet which, by definition, is force

and torque-free. This type of singularity model has been widely used in modelling suspensions of force-free particles (Batchelor 1970) and swimming micro-organisms (Pedley & Kessler 1992; Hatwalne *et al.* 2004; Hernandez-Ortiz *et al.* 2005). The approach is equivalent to considering the swimmer at distances much larger than its intrinsic size, so that its precise geometric structure and the fine details of its swimming protocol are encapsulated in the effective far-field multi-pole structure. The two-dimensional assumption, although idealized and not directly relevant to biological swimmers, allows us to explicitly solve the nonlinear free boundary problem, thereby shedding light on this new mode of locomotion.

Our mathematical approach is inspired by the work of Jeong & Moffatt (1992) who considered surface deformations generated by two counter-rotating cylinders beneath a free surface at low-Reynolds numbers. In an idealized model, the flow generated by the two counter-rotating cylinders is modeled by a single potential dipole located on the axis of symmetry of the deformed free surface. This flow results in symmetric deformations of the interface which are calculated, for a given dipole strength and fluid properties, by means of conformal mapping methods. Notably, the conformal map approach allowed them to produce exact solutions even for large nonlinear deformations of the free surface. Furthermore, their analytical results exhibit remarkable agreement with the experimental data of free surface deformations for different rotation rates of the cylinders. Following in the spirit of Jeong & Moffatt (1992), we also use a conformal map to resolve the shape of the free surface in the flow field generated by the swimmer; the swimmer itself is represented as a superposition of suitable point singularities. The difference here is that we must allow for non-symmetric deformations of the interface and adapt the analysis to admit a stresslet singularity in the fluid, rather than a potential dipole. The point singularity model of the swimmer we adopt is the same as that used in a study of swimming near a no-slip wall by Crowdy & Or (2010). We focus on identifying a steady mode of locomotion in which a swimmer translates at a constant speed parallel to the undisturbed free surface. Since, in the neighbourhood of a flat no-slip wall, the motion of a swimmer generically follows a time-dependent periodic orbit, it is not clear *a priori* that a steadily translating swimmer motion beneath a free capillary surface is possible. What we show below is that such a mode of locomotion is indeed possible and, within our model, can be described in a mathematically explicit way.

This paper is organized as follows. In § 2, the two-dimensional Stokes equations and relevant boundary conditions are introduced using complex variables. The singularity model is then explained in § 3. Section 4 uses a method of images to demonstrate that steady motion of a swimmer beneath a flat, undeformed interface is not possible. Section 5 then introduces a conformal mapping approach that enables us to explore solutions in which the free surface admits essentially arbitrary deformations for any capillary number. Section 6 gives a characterization of the class of steadily translating solutions; the most physically relevant situation is found to be associated with small capillary numbers and small free surface deformations. Section 7 presents a detailed asymptotic analysis of this régime and shows explicitly that steady swimming beneath a free surface results from a subtle interplay between surface tension and interface deformability. Finally, further perspectives are discussed in § 8.

2. Complex variable formulation of Stokes flow

Let the two-dimensional quiescent fluid occupy the area beneath a deformable fluid-air interface, D. The fluid is assumed to be incompressible and, in the Stokes

régime, the streamfunction $\hat{\psi}$ is known to satisfy the biharmonic equation,

$$\nabla^4 \hat{\psi}(\hat{x}, \hat{y}) = 0. \tag{2.1}$$

Introducing the complex-valued coordinate $\hat{z} = \hat{x} + \mathrm{i}\hat{y}$, it is possible to write the general solution of the biharmonic equation in the form,

$$\hat{\psi} = \mathrm{Im}[\bar{\hat{z}}\hat{f}(\hat{z}) + \hat{g}(\hat{z})]. \tag{2.2}$$

Here $\hat{f} \equiv \hat{f}(\hat{z})$ and $\hat{g} \equiv \hat{g}(\hat{z})$ are two functions which must be analytic functions of $\hat{z}$ inside the fluid region except at isolated points where singularities are deliberately introduced in order to model particular flow conditions. These functions are sometimes referred to as *Goursat functions*.

It is possible (Langlois 1964) to express all the usual physical variables in terms of these two functions. Indeed, it can be shown that

$$\left.\begin{aligned} \frac{\hat{p}}{\hat{\mu}} - \mathrm{i}\hat{\omega} &= 4\hat{f}'(\hat{z}), \\ \hat{u} + \mathrm{i}\hat{v} &= -\hat{f}(\hat{z}) + \hat{z}\overline{\hat{f}'(\hat{z})} + \overline{\hat{g}'(\hat{z})}, \\ \hat{e}_{11} + \mathrm{i}\hat{e}_{12} &= \hat{z}\overline{\hat{f}''(\hat{z})} + \overline{\hat{g}''(\hat{z})}. \end{aligned}\right\} \tag{2.3}$$

Here, $\hat{p}$ is the fluid pressure, $\hat{\omega}$ is the vorticity, $(\hat{u}, \hat{v})$ is the fluid velocity and $\hat{e}_{ij}$ is the fluid rate-of-strain tensor. The dynamic fluid viscosity is $\hat{\mu}$. Primes denote differentiation with respect to $\hat{z}$ and overbars denote complex conjugates.

The stress boundary condition on the free surface requires that the normal fluid stress is balanced by the surface tension and that the tangential stress vanishes. This can be written as

$$-\hat{p}n_i + 2\hat{\mu}\hat{e}_{ij}n_j = \sigma\kappa n_i, \tag{2.4}$$

where σ is the surface tension, κ is the surface curvature and n_i is the outward unit vector normal to the interface. In addition, the kinematic condition on the interface requires that the normal velocity of the interface equals the normal fluid velocity.

The governing equations, Goursat functions, and corresponding boundary conditions are non-dimensionalized as follows:

$$\left.\begin{aligned} &\hat{z} = \hat{h}z, \quad \hat{z}_d = \hat{h}z_d, \quad \hat{u} + \mathrm{i}\hat{v} = \hat{U}(u + \mathrm{i}v), \quad \hat{\psi} = \hat{U}\hat{h}\psi, \\ &\hat{f} = \hat{U}f, \quad \hat{g} = \hat{U}\hat{h}g, \quad \hat{p} = \frac{\hat{\mu}\hat{U}}{\hat{h}}p, \end{aligned}\right\} \tag{2.5}$$

where $\hat{z}_d$ is the dimensional location of the swimmer, $\hat{h}$ is the magnitude of $\hat{z}_d$ or the vertical distance of the swimmer from the interface and $\hat{U}$ is a characteristic speed of translation. The capillary number, Ca, which reflects the dimensionless ratio of viscous to capillary effects, is defined as

$$Ca = \frac{\hat{\mu}\hat{U}}{\sigma}. \tag{2.6}$$

It can be shown that the complex form of the stress condition (2.4) on the air–fluid interface is equivalent to the relation

$$\frac{\mathrm{d}H}{\mathrm{d}s} = -\frac{\mathrm{i}}{2Ca}\frac{\mathrm{d}^2 z}{\mathrm{d}s^2}, \tag{2.7}$$

where $\mathrm{d}s$ is a differential element of arc length along the free surface and

$$H \equiv f(z) + z\overline{f}'(\overline{z}) + \overline{g}'(\overline{z}). \tag{2.8}$$

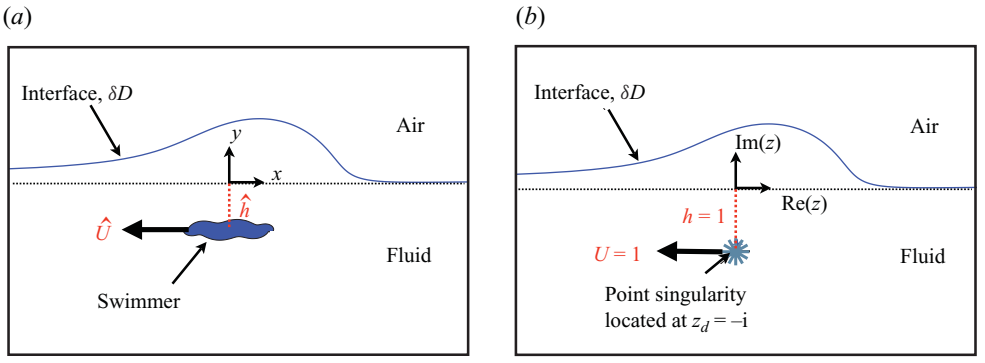

FIGURE 1. (Colour online available at journals.cambridge.org/FLM) Illustration of the singularity model: a finite-area swimmer beneath a free surface is modelled as a point stresslet singularity with superposed potential dipole and quadrupole.

Hence, the stress condition can be integrated once with respect to s to give

$$f(z) + z\overline{f}'(\overline{z}) + \overline{g}'(\overline{z}) = -\frac{\mathrm{i}}{2Ca}\frac{\mathrm{d}z}{\mathrm{d}s}, \tag{2.9}$$

where, without loss of generality, the constant of integration has been set equal to zero.

3. A singularity model of the swimmer

From the first equation in (2.3), it is clear that singularities of the Goursat function $f(z)$ will be related to local singularities in the pressure field and hence, to localized force singularities. A logarithmic singularity of $f(z)$ corresponds to what is often referred to as a *stokeslet*, or point force singularity (Pozrikidis 1992) which, as previously discussed, is not allowed owing to the condition that the swimmer exerts no net force on the flow.

The next order singularity (the derivative of the logarithm) is a simple pole. If near z_d, $f(z)$ has a simple pole singularity,

$$f(z) = \frac{s^*}{z - z_d} + \text{analytic function}, \tag{3.1}$$

then, in order to ensure that the velocity field scales like $1/|z - z_d|$ (rather than $1/|z - z_d|^2$) we must also have

$$g'(z) = \frac{s^*\overline{z_d}}{(z - z_d)^2} + \text{analytic function}. \tag{3.2}$$

Thus, if $f(z)$ and $g'(z)$ locally have the behaviour reflected in (3.1) and (3.2), respectively, near z_d then there is a stresslet of strength s^* at z_d. In general, if $g(z)$ has a simple pole near some point z_d of the form,

$$g(z) = \frac{d}{z - z_d} + \text{analytic function}, \tag{3.3}$$

then we say there is a *dipole* of strength d at z_d. A stresslet singularity of strength s^* at z_d, therefore, corresponds to a simple pole of $f(z)$ at z_d with residue s^* together with a simple pole of $g(z)$ with residue $-s^*\overline{z_d}$ at the same point.

There is a physical way to understand this singularity of $f(z)$. Swimmers at low-Reynolds numbers propel themselves by exerting a local force on the flow (for example, the waving flagellum of a spermatozoa) which is then counterbalanced by a net drag on its body (the head of the spermatozoa plus its flagellum) leaving the total net force on it equal to zero (e.g. see review in Lauga & Powers 2009). If this scenario is modeled as two logarithmic singularities of $f(z)$ (two point forces) drawing infinitesimally close together with equal and opposite strengths tending to infinity at a rate inversely proportional to their separation, the limit is precisely a simple pole singularity of $f(z)$ of the form (3.1).

In a general singularity description of a swimmer, $g'(z)$ is also singular at z_d. We already know it must have a second-order pole (3.2) (this is associated with the stresslet) but it can have additional singularities. The singularities of $g(z)$ are potential multi-poles because, as is clear from (2.3), only the singularities of $f(z)$ contribute to the vorticity of the flow. Different swimmers generate different effective singularities according to their particular swimming protocol. Any choice of singularities that we assume $g'(z)$ to have at z_d is, therefore, a manifestation of our choice of swimmer type. It is not clear, *a priori*, how to pick either the type of these singularities of $g'(z)$ or their magnitudes.

In this paper, we adopt the same singularity model of a swimmer used by Crowdy & Or (2010) in their studies of a low-Reynolds number swimmer near a no-slip wall. They motivated their choice of singularities by considering a concrete model of a finite-area circular 'treadmilling' swimmer of radius ϵ. It was supposed that, on its surface, the swimmer generates a purely tangential surface velocity given by

$$U(\phi, t) = 2V \sin(2(\phi - \theta(t))), \tag{3.4}$$

where V is a constant (setting the time scale of the swimmer's motion), ϕ is the angular variable and $\theta(t)$ is a distinguished angle taken to be the direction in which the head of the swimmer is pointed. By solving a boundary value problem for the flow associated with this swimmer in an unbounded Stokes flow, it is possible to show that such a swimmer has an effective singularity description consisting of a stresslet of strength $\mu(t) = \epsilon V \exp(2\mathrm{i}\theta(t))$ with a superposed potential quadrupole of strength $2\mu(t)\epsilon^2$.

This model is a particular case of a general class of simplified swimmers first considered in a theoretical study due to Blake (1971*b*) who looked at the effect of imposing velocity profiles of general form on the surface of a circular swimmer. Such an 'envelope model' captures the macroscopic effect of the motion of many small-scale beating cilia on the swimmer surface. Similarly, cilia-aided crawling of organisms beneath a free surface has been observed in nature, in particular for some families of snails. Copeland (1919) concluded that the locomotion of *Alectrion trivittata*, which crawls upside down on the surface, relies solely on the ciliary action. He conducted a similar study on *Polinices duplicata* and *Polinices heros*, both of which were observed to use both cilia and muscle contraction for locomotion on hard surfaces (Copeland 1922). Only ciliary motion was employed by the young *Polinices heros* when crawling inverted beneath the surface.

Prompted by the success of the previously described singularity model, we extend the study to point swimmers (beneath a free surface) within the same general class: that is, a point stresslet superposed with a potential dipole and quadrupole (see Figure 1). The dipole has been included because it is a lower order singularity than the quadrupole and there is no reason *a priori* to suppose it is absent (moreover steady rectilinear motion is expected to involve a dipole in its singularity description).

This means that we will seek $f(z)$ and $g(z)$ with the functional forms,

$$f(z) = \frac{s^*}{z+\mathrm{i}} + f_0 + f_1(z+\mathrm{i}) + \cdots, \quad g(z) = \frac{q^*}{(z+\mathrm{i})^2} + \frac{(-\mathrm{i}s^* + d^*)}{(z+\mathrm{i})} + g_0 + g_1(z+\mathrm{i}) + \cdots, \tag{3.5}$$

where the singularity is at $z = -\mathrm{i}$ and f_0, f_1, g_0 and g_1 are constants. We will refer to s^* as the stresslet strength, q^* as the quadrupole strength and d^* as the dipole strength (note that part of the coefficient of $1/(z+\mathrm{i})$ in $g(z)$ is naturally associated with the stresslet singularity as seen in (3.1) and (3.2)). We will not make any *a priori* assumptions on the relative magnitudes of s^*, d^* and q^* since, for a steady solution, we expect these to be determined by the conditions for equilibrium.

Crowdy & Or (2010) show that the evolution equations for the swimmer position $z_d(t)$ and its orientation $\theta(t)$ are given by the dynamical system,

$$\frac{\mathrm{d}z_d(t)}{\mathrm{d}t} = -f_0 + z_d\overline{f_1} + \overline{g_1}, \quad \frac{\mathrm{d}\theta(t)}{\mathrm{d}t} = -2\mathrm{Im}[f_1]. \tag{3.6}$$

The first equation states that the swimmer moves with the finite part of the fluid velocity at the swimmer position, while the second equation states that its angular velocity equals half the regular part of the vorticity at the swimmer position. In the present paper, we adopt these same evolution equations but focus on finding equilibrium solutions in which the swimmer translates steadily in the direction of the undeformed interface (i.e. parallel to the x-axis). In a co-travelling frame, we therefore need to find solutions satisfying the conditions

$$0 = -f_0 + z_d\overline{f_1} + \overline{g_1}, \quad 0 = \mathrm{Im}[f_1]. \tag{3.7}$$

The first equation ensures that the swimmer is stationary in the co-moving frame; the second ensures that the local vorticity at the swimmer position vanishes so that its orientation remains fixed in time. For swimmers near a no-slip wall, it should be noted that the time evolution of the swimmer's orientation proves to be a crucial ingredient in understanding the swimmer dynamics (Berke *et al.* 2008), and the same is expected to be true near a free surface.

4. Steady swimming beneath a flat interface: method of images

It is instructive to first examine whether it is possible to find a solution for a point swimmer of the type just described translating steadily beneath a flat undeformed interface. To do so we must seek $f(z)$ and $g(z)$ satisfying the boundary conditions on the free surface, with singularities of the form (3.5) and satisfying conditions (3.7). Owing to the simplicity of the geometry, we search for such a solution using the method of images, as originally introduced by Blake and co-workers for three-dimensional flows near no-slip walls (Blake 1971*a*; Blake & Chwang 1974). We will demonstrate that such a solution does not exist. In subsequent sections, we succeed in identifying steadily translating solutions when the interface deforms. This highlights the indispensable role played by the deformability of the interface in providing a mechanism for steady translation of the swimmer.

Consider a swimmer moving at a prescribed horizontal speed $U = -1$ beneath a flat interface in a Stokes flow with no background flow. It is convenient to work in a frame travelling with the swimmer. Then the swimmer is stationary at $z_d = -\mathrm{i}$, while the fluid in the far-field has unit speed in the x-direction.

We seek a solution of the form

$$f(z) = \frac{s^*}{z+\mathrm{i}} + \frac{\hat{s^*}}{z-\mathrm{i}} + f_\infty, \tag{4.1}$$

where, in addition to the stresslet of strength s^* at $z_i = -\mathrm{i}$, we have placed an image stresslet of strength $\hat{s^*}$ (to be determined) at $z = \mathrm{i}$ and f_∞ is a constant. The form of $g'(z)$ is now forced by the stress boundary condition on this interface. On $\bar{z} = z$ we have, from (2.9),

$$\overline{g}'(z) = -f(z) - z\overline{f}'(z) + \frac{\mathrm{i}}{2Ca}\cdot \tag{4.2}$$

Substitution of (4.1) into (4.2) and picking $\hat{s^*} = \overline{s^*}$ so that $g'(z)$ has no rotlet contribution (no simple poles) leads to

$$g'(z) = -\frac{\mathrm{i}s^*}{(z+\mathrm{i})^2} + \frac{\mathrm{i}\overline{s^*}}{(z-\mathrm{i})^2} + g_\infty, \tag{4.3}$$

which we rewrite as

$$g'(z) = \left[\frac{\mathrm{i}s^*}{(z+\mathrm{i})^2} - \frac{\mathrm{i}\overline{s^*}}{(z-\mathrm{i})^2}\right] - \frac{2\mathrm{i}s^*}{(z+\mathrm{i})^2} + \frac{2\mathrm{i}\overline{s^*}}{(z-\mathrm{i})^2} + g_\infty. \tag{4.4}$$

As can be seen by comparison of (4.1) and (4.4) with (3.1) and (3.2), the two second-order poles in square brackets are associated with the two stresslets – the swimmer stresslet and its image – and the additional second-order poles correspond to superposed potential dipole singularities, one at the swimmer position and another at the image point.

The constants f_∞ and g_∞ must be picked so that the far-field velocity condition is satisfied. Making use of (4.1) and (4.2) in the expression for the velocity (2.3) in the far-field equation produces

$$-f_\infty + \overline{g_\infty} = 1. \tag{4.5}$$

By balancing the constant terms in the stress condition, we can deduce

$$f_\infty = -\frac{1}{2} + \frac{\mathrm{i}}{4Ca}, \quad g_\infty = \frac{1}{2} - \frac{\mathrm{i}}{4Ca}\cdot \tag{4.6}$$

Finally, the swimmer must be stationary in the co-translating frame. Hence the finite part of

$$-f(z) + z\overline{f}'(\bar{z}) + \overline{g}'(\bar{z}) \tag{4.7}$$

at $z = -\mathrm{i}$ must vanish. This leads to

$$0 = -\frac{\overline{s^*}}{(-2\mathrm{i})} - f_\infty + \frac{\mathrm{i}s^*}{(-4)} - \frac{\mathrm{i}s^*}{(-4)} + \overline{g_\infty} \tag{4.8}$$

and the conclusion that

$$s^* = 2\mathrm{i}. \tag{4.9}$$

It is not surprising that the strength of these singularities does not depend on the capillary number since we have stipulated that the interface is flat and hence do not expect surface tension to play a role in the dynamics.

The solutions for $f(z)$ and $g'(z)$ just derived give the instantaneous velocity field; we must also check that the free surface is a streamline. It can be verified (see the discussion in the next section) that this condition is equivalent to

$$g(z) + \bar{z}f(z) = 0 \tag{4.10}$$

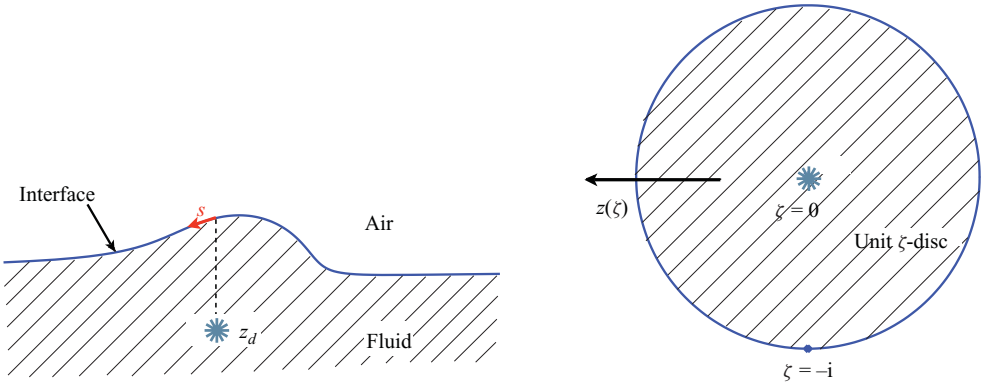

FIGURE 2. (Colour online) Conformal mapping $z(\zeta)$ from the unit ζ-disc to the fluid region beneath the interface. In this mapping, $\zeta = 0$ maps to the swimmer at $z = z_d$, and $\zeta = -\mathrm{i}$ maps to the interface at infinity. The variable s denotes the arclength and increases as shown in the figure.

on the real axis. By making use of (4.1) and (4.2), we find

$$g(z) + zf(z) = \frac{\mathrm{i}s^*}{(z+\mathrm{i})} - \frac{\mathrm{i}\overline{s^*}}{(z-\mathrm{i})} + zg_\infty + \frac{zs^*}{(z+\mathrm{i})} + \frac{z\overline{s^*}}{(z-\mathrm{i})} + zf_\infty$$
$$= 2\mathrm{Re}[s^*] = 0, \tag{4.11}$$

which confirms that the free surface is indeed a streamline. Re indicates the real part.

The functions $f(z)$ and $g(z)$ will have local expansions, near the swimmer, of the form (3.5) and it still remains to satisfy the condition $\mathrm{Im}[f_1] = 0$, as in (3.7). But it is easily verified that this condition is not satisfied identically and, furthermore, there are no remaining degrees of freedom that will allow us to enforce it. It is therefore concluded that solutions for a non-rotating, steadily translating swimmer beneath a flat interface do not exist.

5. Steady swimming beneath a deformed interface: conformal mapping

This failure to find a steady solution beneath an undeformed interface does not preclude the existence of such solutions when the interface deforms. We now seek such solutions. When the interface is deformed, it is no longer clear how to apply the method of images. Instead, we introduce a new solution method based on conformal mapping. It enables us to resolve the nonlinear interaction between the point swimmer and the deformed free surface in analytical form.

Consider the unit disc $|\zeta| \leqslant 1$ in a complex parametric ζ-plane. It is known, by the Riemann mapping theorem (Ablowitz & Fokas 1997), that there exists a conformal mapping $z(\zeta)$ that will map this unit disc to the fluid region beneath the free surface. The free surface itself will be the image of the unit circle $|\zeta| = 1$ under this mapping (see figure 2). Since the physical fluid domain is unbounded and the free surface extends to infinity, there must be a simple pole of $z(\zeta)$ on the unit ζ-circle. Using a rotational degree of freedom of the Riemann mapping theorem, we take this pole to be at $\zeta = -\mathrm{i}$. The most general form of the mapping can then be represented as

$$z(\zeta) = \frac{a}{\zeta + \mathrm{i}} + \sum_{k=0}^{\infty} a_k \zeta^k, \tag{5.1}$$

where a and $\{a_k\}$ are a (generally infinite) set of complex coefficients. For a one-to-one function, it must also be true that $\mathrm{d}z/\mathrm{d}\zeta \neq 0$ inside the unit disc. There are two remaining degrees of freedom in the mapping theorem which allow us to prescribe that the singularity z_d corresponding to the swimmer is the image of $\zeta = 0$, i.e.

$$z_d = z(0). \tag{5.2}$$

This means that the pre-image of z_d is the point $\zeta = 0$.

We seek a solution where the singularity travels uniformly with speed $U = -1$ in the x-direction and we again move to a co-travelling frame in which both the swimmer and the shape of the free surface are stationary. The kinematic condition on the interface for a steady solution in this frame is

$$\boldsymbol{u}\cdot\boldsymbol{n} = 0. \tag{5.3}$$

If the normal vector is $\boldsymbol{n} = (n_x, n_y)$, the complex normal $n_x + \mathrm{i}n_y$ is equal to $-\mathrm{i}\mathrm{d}z/\mathrm{d}s$, where s increases along the interface from positive infinity to negative (see figure 2). Using this fact, (5.3) can be expressed in the complex form as

$$\mathrm{Re}\left[(u + \mathrm{i}v)\mathrm{i}\frac{\mathrm{d}\overline{z}}{\mathrm{d}s}\right] = 0. \tag{5.4}$$

This condition is equivalent to the free surface being a streamline and, in turn, corresponds to the following condition at the free surface:

$$\overline{z}f(z) + g(z) = 0. \tag{5.5}$$

The easiest way to show this is to compute the derivative, with respect to arclength s, of the quantity $\overline{z}f(z) + g(z)$ on the interface and then make use of (2.9) and (5.4) to show that $\overline{z}f(z) + g(z)$ is constant and, without loss of generality, equal to zero.

In the far-field it is required that

$$f(z) \to f_\infty + \frac{f_\infty^{(1)}}{z} + \cdots \quad \text{and} \quad g'(z) \to g_\infty + \frac{g_\infty^{(1)}}{z} + \cdots \tag{5.6}$$

so that, as $z \to \infty$,

$$u + \mathrm{i}v \to -f_\infty + \overline{g_\infty} + O(|z|^{-1}). \tag{5.7}$$

To satisfy the boundary conditions at infinity that the interface moves in the x-direction with unit speed, we must have

$$-f_\infty + \overline{g_\infty} = 1. \tag{5.8}$$

It can be shown that

$$f_\infty = -\frac{1}{2} + \frac{\mathrm{i}}{4Ca} \quad \text{and} \quad g_\infty = \frac{1}{2} - \frac{\mathrm{i}}{4Ca}. \tag{5.9}$$

To see how these relations arise, we make use of the fact that

$$\frac{\mathrm{d}z}{\mathrm{d}s} = \frac{\mathrm{i}\zeta z_\zeta}{|z_\zeta|}, \tag{5.10}$$

and show that, as $\zeta \to -\mathrm{i}$,

$$-\frac{\mathrm{i}}{2}\frac{\mathrm{d}z}{\mathrm{d}s} \to \frac{\mathrm{i}}{2Ca}\frac{a}{|a|}, \tag{5.11}$$

so that, using the condition (2.9), as $\zeta \to -\mathrm{i}$,

$$f_\infty + \overline{g_\infty} = \frac{\mathrm{i}}{2Ca}\frac{a}{|a|}. \tag{5.12}$$

Since, as $\zeta \to -\mathrm{i}$ on $|\zeta| = 1$,

$$\overline{z} = \overline{z}(\zeta^{-1}) = \frac{\overline{a}\zeta}{1-\mathrm{i}\zeta} + \overline{a_0} + \frac{\overline{a_1}}{\zeta} = \frac{\overline{a}}{\zeta+\mathrm{i}} + \mathrm{i}\overline{a} + \overline{a_0} + \frac{\overline{a_1}}{\zeta} \to \frac{\overline{a}z}{a} + \cdots, \tag{5.13}$$

it also follows, from (5.5), that

$$g(z) \to -\frac{f_\infty \overline{a} z}{a}, \tag{5.14}$$

and hence

$$g_\infty = -\frac{f_\infty \overline{a}}{a}. \tag{5.15}$$

This means, from (5.8), that

$$-f_\infty - \frac{\overline{f_\infty} a}{\overline{a}} = 1. \tag{5.16}$$

The only way for the velocity to be purely real is for a to be real so that

$$-f_\infty - \overline{f_\infty} = 1. \tag{5.17}$$

It further follows, from (5.12), that

$$f_\infty - \overline{f_\infty} = \frac{\mathrm{i}}{2Ca}, \tag{5.18}$$

leading to (5.9). Together with the stress condition (2.9), the kinematic condition (5.3) can be written as

$$\mathrm{Re}\left[2f\mathrm{i}\overline{\left(\frac{\mathrm{d}z}{\mathrm{d}s}\right)}\right] = \frac{1}{2Ca}. \tag{5.19}$$

We now introduce the composed functions

$$F(\zeta) \equiv f(z(\zeta)), \quad G(\zeta) \equiv g(z(\zeta)), \tag{5.20}$$

which can be used in the kinematic condition together with (5.10) to give

$$\mathrm{Re}\left[\frac{2F(\zeta)}{\zeta z_\zeta}\right] = \frac{1}{2Ca|z_\zeta|}, \tag{5.21}$$

where $z_\zeta(\zeta) \equiv \mathrm{d}z/\mathrm{d}\zeta$. Since $f(z)$ is required to have a simple pole at z_d, $F(\zeta)$ must have a simple pole at $\zeta = 0$. Therefore, near $\zeta = 0$,

$$F(\zeta) = \frac{F_d}{\zeta} + F_0 + O(\zeta), \tag{5.22}$$

for some constant F_d to be determined. Therefore, consider

$$\mathrm{Re}\left[\frac{F(\zeta)}{\zeta z_\zeta} - \frac{D}{\zeta^2} - \frac{C}{\zeta}\right] = \frac{1}{4Ca|z_\zeta|} - \mathrm{Re}\left[\frac{D}{\zeta^2} + \frac{C}{\zeta}\right] = \frac{1}{4Ca|z_\zeta|} - \mathrm{Re}\left[\overline{D}\zeta^2 + \overline{C}\zeta\right]. \tag{5.23}$$

For suitable choices of constants C and D, the function in the square brackets on the left-hand side of (5.23) is analytic everywhere inside the unit ζ-disc. Equation (5.23)

therefore gives the real part of an analytic function on the boundary of the disc. The Poisson integral formula can be used to give

$$F(\zeta) = \zeta z_\zeta(\zeta)\left[I(\zeta, Ca) + \frac{D}{\zeta^2} + \frac{C}{\zeta} - \overline{D}\zeta^2 - \overline{C}\zeta + \mathrm{i}b\right], \tag{5.24}$$

where b is some real constant and

$$I(\zeta, Ca) = \frac{1}{8\pi \mathrm{i} Ca}\oint_{|\zeta'|=1} \frac{\mathrm{d}\zeta'}{\zeta'}\frac{\zeta'+\zeta}{\zeta'-\zeta}\frac{1}{|z_\zeta(\zeta')|}. \tag{5.25}$$

Since $z_\zeta(\zeta)$ has a second-order pole at $\zeta = -\mathrm{i}$, it is necessary that the quantity inside the brackets in expression (5.24), and its derivative, vanish at $\zeta = -\mathrm{i}$ so that near $\zeta = -\mathrm{i}$,

$$I(\zeta, Ca) + \frac{D}{\zeta^2} + \frac{C}{\zeta} - \overline{D}\zeta^2 - \overline{C}\zeta + \mathrm{i}b = A(\zeta + \mathrm{i})^2 + \cdots \tag{5.26}$$

for some complex constant A which is related to f_∞ by

$$\mathrm{i}aA = f_\infty. \tag{5.27}$$

This means that

$$I(-\mathrm{i}, Ca) - D + \overline{D} + \mathrm{i}C + \mathrm{i}\overline{C} + \mathrm{i}b = 0, \tag{5.28}$$

and

$$I_\zeta(-\mathrm{i}, Ca) + 2\mathrm{i}D + C + 2\overline{D}\mathrm{i} - \overline{C} = 0, \tag{5.29}$$

while

$$A = \tfrac{1}{2}\left[I_{\zeta\zeta}(-\mathrm{i}, Ca) + 6D - 2C\mathrm{i} - 2\overline{D}\right]. \tag{5.30}$$

Since $I(-\mathrm{i}, Ca)$ is purely imaginary, (5.28) is a single real condition, namely, an equation for the real parameter b in terms of C and D.

If the map $z(\zeta)$ and the constants b, C and D are known, (5.24) gives an explicit expression for $F(\zeta)$. Condition (5.5) then provides the following expression for $G(\zeta)$:

$$G(\zeta) = -\overline{z}(\zeta^{-1})F(\zeta). \tag{5.31}$$

This condition is very revealing: it shows that the singularities of $G(\zeta)$ dictate the singularities of the conformal mapping function $z(\zeta)$. In particular, it shows that if $G(\zeta)$ has a pole singularity at $\zeta = 0$ then the functional form of the mapping function has a finite representation. To see this suppose, for example, that $z(\zeta)$ has the special truncated form,

$$z(\zeta) = \frac{a}{\zeta + \mathrm{i}} + a_0 + \sum_{k=1}^{n} a_k \zeta^k, \tag{5.32}$$

where $n \geqslant 1$ is some positive integer. Then

$$\overline{z}(\zeta^{-1}) = \frac{\overline{a}\zeta}{1 - \mathrm{i}\zeta} + \overline{a_0} + \sum_{k=1}^{n} \frac{\overline{a_k}}{\zeta^k}. \tag{5.33}$$

Since $F(\zeta) = O(\zeta^{-1})$ as $\zeta \to 0$, it follows from (5.31) and (5.33) that, near $\zeta = 0$, $G(\zeta)$ has the form

$$G(\zeta) = \frac{G_{-(n+1)}}{\zeta^{n+1}} + \frac{G_{-n}}{\zeta^n} + \cdots + \frac{G_{-1}}{\zeta} + G_0 + G_1\zeta + \cdots \tag{5.34}$$

implying that, near z_d,

$$g(z) = \frac{g_{-(n+1)}}{(z - z_d)^{n+1}} + \text{higher order terms.} \tag{5.35}$$

Since our swimmer model means that $g(z)$ must have the form given in (3.5), it is clear that we must pick $n = 1$. The conformal map then has the form

$$z(\zeta) = \frac{a}{\zeta + \mathrm{i}} + a_0 + a_1\zeta, \tag{5.36}$$

where a, a_0 and a_1 are complex numbers.

In addition, there are geometrical constraints on the conformal mapping parameters. Suppose that the singularity is at $z_d = -\mathrm{i}$. This implies that $z(0) = -\mathrm{i}$ and therefore that

$$a_0 = (a - 1)\mathrm{i}. \tag{5.37}$$

Furthermore, the condition that the interface tends to $y = 0$ implies

$$\mathrm{Re}[a_1] = \frac{a}{2} - 1. \tag{5.38}$$

Hence, the mapping function can be expressed as

$$z(\zeta) = \frac{a}{\zeta + \mathrm{i}} + \mathrm{i}(a - 1) + \left(\frac{a}{2} - 1 + \mathrm{i}c\right)\zeta, \tag{5.39}$$

where a and c are two real parameters. These two parameters have the following geometrical interpretations. When $a = 2$ with $c = 0$ the interface is flat; increasing a above 2 corresponds to a symmetric *upward* deformation of the interface; decreasing a below 2 leads to a symmetric *downward* deformation. Changing the value of c away from zero introduces left–right *asymmetry* of the free surface deformation about a vertical axis through the swimmer, as illustrated in figure 3.

The velocity of the swimmer in the co-moving frame is given by the finite part of the expression $u + \mathrm{i}v$ at $z = -\mathrm{i}$ and, for a steady solution, this must vanish. If

$$f(z) = \frac{s^*}{z + \mathrm{i}} + f_0 + f_1(z + \mathrm{i}) + \cdots, \quad g(z) = \frac{q^*}{(z + \mathrm{i})^2} + \frac{(-\mathrm{i}s^* + d^*)}{(z + \mathrm{i})} + g_0 + g_1(z + \mathrm{i}) + \cdots, \tag{5.40}$$

the finite part of $u + \mathrm{i}v$ at $z = -\mathrm{i}$ is given by

$$-f_0 - \mathrm{i}\overline{f_1} + \overline{g_1} = 0. \tag{5.41}$$

The terms f_0, f_1 and g_1 are given (using the residue theorem) as

$$\left.\begin{aligned} f_0 &= \frac{1}{2\pi\mathrm{i}} \oint_\Gamma \frac{F(\zeta)}{(z(\zeta) + \mathrm{i})} \frac{\mathrm{d}z}{\mathrm{d}\zeta}\, \mathrm{d}\zeta, \qquad f_1 = \frac{1}{2\pi\mathrm{i}} \oint_\Gamma \frac{F(\zeta)}{(z(\zeta) + \mathrm{i})^2} \frac{\mathrm{d}z}{\mathrm{d}\zeta}\, \mathrm{d}\zeta, \\ g_1 &= -\frac{1}{2\pi\mathrm{i}} \oint_\Gamma \frac{\overline{z}(1/\zeta)F(\zeta)}{(z(\zeta) + \mathrm{i})^2} \frac{\mathrm{d}z}{\mathrm{d}\zeta}\, \mathrm{d}\zeta, \end{aligned}\right\} \tag{5.42}$$

where Γ is any simple closed curve surrounding $\zeta = 0$. Note that with $F(\zeta)$ determined from (5.24), $G(\zeta)$ from (5.31) and f_0, f_1 and g_1 from (5.42), condition (5.41) is a linear equation in the constants C and D. It should also be pointed out that f_0, f_1 and g_1 can, in principle, be found in analytical form but the algebra involved is lengthy and it is easier to make use of the integral expressions (5.42) to compute these quantities.

If the values of a, c and U are specified, C and D can be found by simultaneously solving

$$-f_0 - \mathrm{i}\overline{f_1} + \overline{g_1} = 0, \tag{5.43}$$

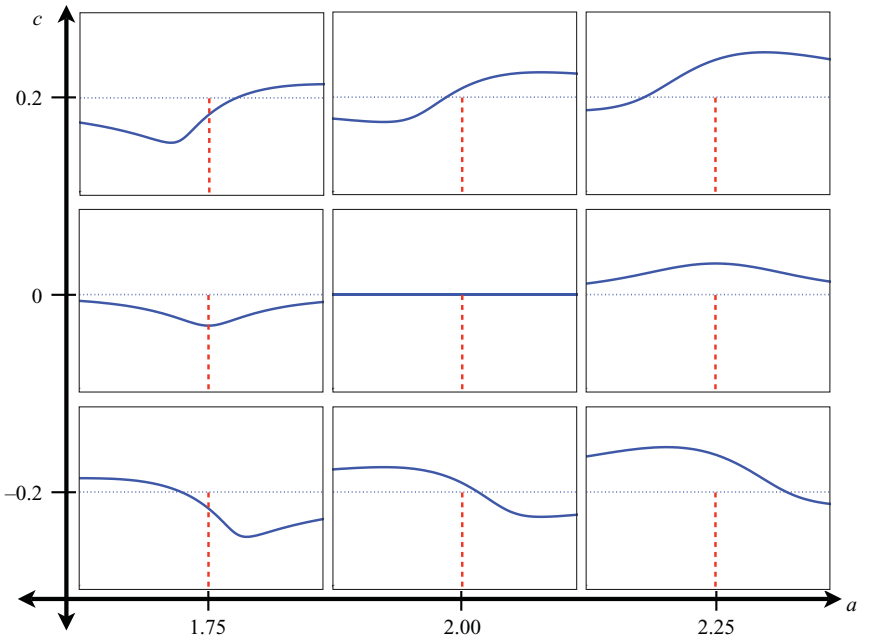

FIGURE 3. (Colour online) The geometrical interpretation of the parameters a and c. The flat interface corresponds to $a=2, c=0$. Increasing (decreasing) a above 2 with $c=0$ (along the horizontal axis) moves the interface up (down) in a left–right symmetric fashion. Non-zero values of c (along the vertical axis) introduce left–right asymmetry.

which is a complex equation, together with the real equation (5.29), i.e.

$$I_\zeta(-\mathrm{i}, Ca) + 2\mathrm{i}D + C + 2\overline{D}\mathrm{i} - \overline{C} = 0, \tag{5.44}$$

and the real equation

$$-\frac{1}{2} = \mathrm{Re}\left[\frac{\mathrm{i}a}{2}\left[I_{\zeta\zeta}(-\mathrm{i}, Ca) + 6D - 2C\mathrm{i} - 2\overline{D}\right]\right]. \tag{5.45}$$

With constants C and D determined in this way, functions $F(\zeta)$ and $G(\zeta)$, and hence the flow field, are fully determined in analytical form. The stresslet, dipole and quadrupole strengths can then be readily computed to be

$$\left.\begin{aligned} s^* &= D\left(\frac{3a-2}{2} + \mathrm{i}c\right)^2, \\ q^* &= -D\left(\frac{a-2}{2} - \mathrm{i}c\right)\left(\frac{3a-2}{2} + \mathrm{i}c\right)^2, \\ d^* &= \left(\frac{3a-2}{2} + \mathrm{i}c\right)\left[\mathrm{i}Da\left(-\frac{a}{2} + 3 + 5\mathrm{i}c\right)\right. \\ &\quad \left. -C\left(\frac{a-2}{2} - \mathrm{i}c\right)\left(\frac{3a-2}{2} + \mathrm{i}c\right)\right]. \end{aligned}\right\} \tag{5.46}$$

As a check on the solution scheme, it was verified that when $a=2, c=0$ (so that the interface is flat), we retrieved the values

$$s^* = 2\mathrm{i}, \quad d^* = -4, \quad q^* = 0, \tag{5.47}$$

which are the values obtained in § 4 using the method of images.

We have thus found that there is a two-parameter family of solutions, parametrized by a and c, for a force-free (but not necessarily non-rotating) point swimmer – characterized by a singularity description of the form (3.5) – steadily translating beneath a deformed free surface with speed $U=-1$.

It remains, however, to enforce the condition $\mathrm{Im}[f_1]=0$. In contrast to the case when the interface is assumed to be flat, we now have additional freedoms in the choice of a and c that can potentially be used to enforce this condition. With a two-parameter family of possible solutions, and only a single additional requirement, we choose to specify a and explore if there are values of c such that $\mathrm{Im}[f_1]=0$. It must also then be checked *a posteriori* that the map (5.39) with these values of a and c is a one-to-one mapping to the fluid region. It has been found that such solutions do indeed exist and will be described in the next section.

6. Characterization of the steady solutions

For a given value of a, admissible values of c are found by stipulating that

$$\mathrm{Im}[f_1]=0. \tag{6.1}$$

The nature of the formulation is such that the only stage at which it is necessary to solve a nonlinear equation is in satisfying (6.1). Newton's method is used to satisfy this condition by fixing a value of a and Ca, taking a guess for c and then computing the associated functions $F(\zeta)$ and $G(\zeta)$ together with the values of f_0, f_1 and g_1. The value of c is updated iteratively until condition (6.1) is satisfied. It is checked, *a posteriori*, that the resulting conformal mapping is a one-to-one mapping from the unit ζ-disc to the fluid domain. In this way, we find that equilibrium solutions do indeed exist.

Physically, the relevant values of the capillary number, Ca, are likely to be smaller than unity. For low-Reynolds number biological organisms, Ca will depend on both the size of the organism and the material properties of the environment. In water, where $\mu\approx 0.01$ poises, $\sigma\approx 72$ dynes/cm, typical swimming speeds for micro-organisms such as spermatozoa and the green algae *Chlamydomonas* are on the order of 100 μm/s, corresponding to a capillary number of 1.4×10^{-6}. Although much smaller capillary numbers can easily be realized by smaller microbes (e.g. *E. coli*), 10^{-6} can be considered a rough upper bound on Ca for organisms in water relevant to our analysis, as larger (and hence faster) organisms violate our low-Reynolds number assumption. In contrast, micro-organisms in the body are often surrounded by media significantly more viscous than water. For example, spermatozoa are generally immersed in cervical mucus which has an apparent viscosity ranging from 200–1200 poises (Clift & Hart 1953), corresponding to a capillary number of order 1. Therefore we focus on capillary numbers that are smaller than unity.

Figure 4 shows a graph of c as a function of a for $Ca=0.03$, 0.01 and 0.001. For each of these values of Ca two solution branches are found: that is, for a given value of a within a certain window, solutions satisfying (6.1) with both a positive and a negative value of c are found. When $Ca=0.03$ figure 4 shows that the solution branches are far removed from the flat state solution $a=2, c=0$; indeed, figure 5 shows some typical free surface shapes in this case. When $c>0$ the free surface is more deformed to the left of the swimmer, while for $c<0$ the free surface is more deformed to the right. Both solution branches for $Ca=0.03$ are highly nonlinear and are unlikely to be available from a small-deformation analysis about the flat state (see § 7). It is therefore of significance that these solution branches can be found using the

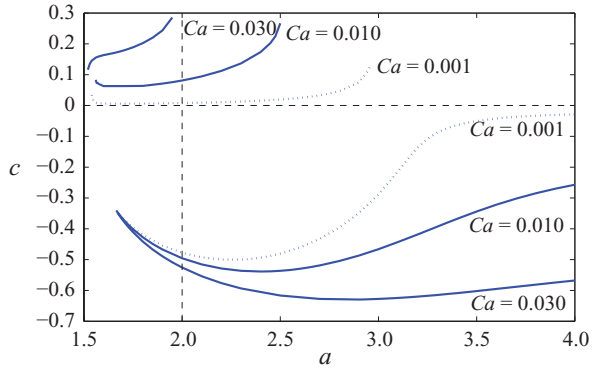

FIGURE 4. (Colour online) Graphs of c against a for $Ca = 0.03$, 0.01 and 0.001; in each case, two distinct solution branches are found. The branch with $c > 0$ becomes close to the flat state as $Ca \to 0$.

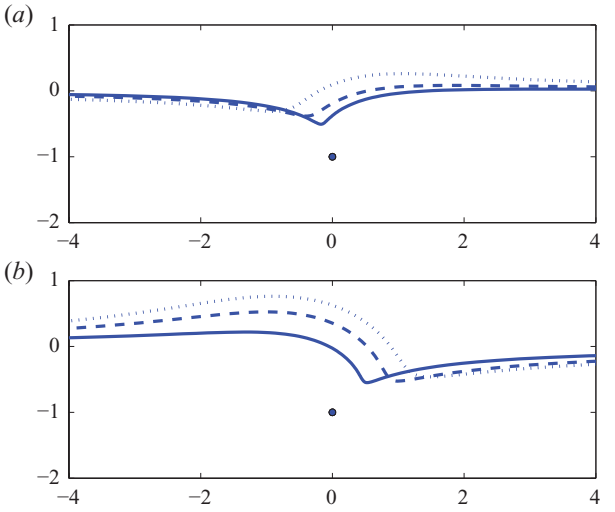

FIGURE 5. (Colour online) Free surface profiles with $Ca = 0.03$. (a) The solutions with $(a, c) = (1.52, 0.116)$ (solid), $(1.7, 0.178)$ (dashed) and $(1.95, 0.285)$ (dotted); (b) solutions with $(a, c) = (1.67, -0.347)$ (solid), $(2, -0.526)$ (dashed) and $(2.3, -0.593)$ (dotted).

complex variable approach adopted here. For all values of Ca considered the branch of solutions with $c < 0$ appears to exist for any choice of a above a minimum value of $a \approx 1.67$ below which no solutions on this branch could be found (in the sense that the Newton iteration to find c-values for which $\mathrm{Im}[f_1] = 0$ failed to converge even for very small decreases in a). The branches of solutions with $c > 0$ are found to exist within particular intervals; for example, for $Ca = 0.03$ solutions exist for $a \in [1.52, 1.95]$.

The nature of the solutions at the edges of these parameter windows is not found to be associated with free surface shapes exhibiting any limiting forms such as near-cusps as found, for example, in the free surface Stokes flows problem studied by Jeong & Moffatt (1992). Such near-cusp formation is, however, usually associated with the limit $Ca \to \infty$ which is not of relevance to our study. It is interesting to point out, however, that our work here has some mathematical connections with that of Jeong

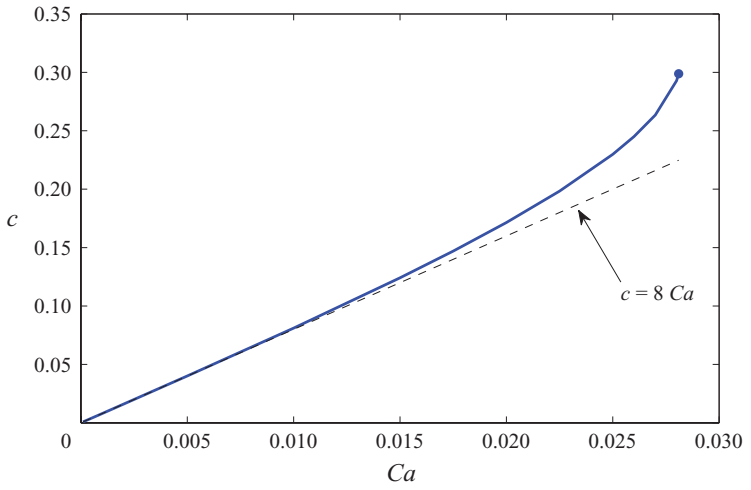

FIGURE 6. (Colour online) Graphs of c against Ca for $a = 2$ on the upper branch with $c > 0$. This branch is found to terminate at $Ca \gtrsim 0.0281$. The asymptotic result (7.11) is also shown.

(1999) who generalized the work in Jeong & Moffatt (1992) to find non-symmetric free surface deformation due to a general vortex dipole situated beneath the free surface. The class of free surface profiles relevant in that case turn out to be exactly the same as those relevant here, although for rather different physical reasons. Jeong (1999) parametrizes his conformal mappings in terms of two parameters (a, b) which can be shown to be mapped to our parameters (a, c) under the transformation of parameters,

$$a \mapsto \frac{a}{2} - 1, \quad b \mapsto c. \tag{6.2}$$

Jeong (1999) goes on to characterize a critical hyperbola in his (a, b)-space at which cusps form on the interface; the corresponding values of (a, c) giving solutions to the steady swimmer problem are found to be well away from this critical hyperbola for all values of Ca considered here.

If we fix $a = 2$ an inspection of the upper branch solutions in figure 4 suggests that there will exist a solution on the upper branch with $c > 0$ for a range of capillary numbers up to some maximum Ca in the interval $0.01 < Ca < 0.03$. Figure 6 shows a graph of the solutions for c against Ca for $a = 2$; the critical value is found to be $Ca \approx 0.0281$. Figures 4 and 6 both show that, as Ca decreases, the upper solution branch with $c > 0$ tends down towards the a-axis, so that $c \to 0$, with solutions existing in a neighbourhood of $a = 2$. This means that solutions on the upper branches with $a \approx 2$ draw close to, but not equal to, the flat state solution as Ca decreases. The lower solution branches with $c < 0$, on the other hand, appear to remain well removed from the flat state solution and are qualitatively similar to the $c < 0$ solution branch when $Ca = 0.03$. Figure 7 shows typical free surface profiles for $Ca = 0.001$: a solution close to the flat state, with $(a, c) = (2, 0.008)$, is clearly shown. The multi-pole strengths are generally complex but figure 8 shows their magnitudes, $|s^*|$, $|d^*|$ and $|q^*|$, as a function of a on both solution branches. It reveals that, for most of the solutions, the multi-pole strengths appear to be large; for example, on the lower branch they are typically of order 10^2 and 10^3. Indeed, only solutions on the upper $c > 0$ branch with $a \approx 2$ and $c \approx 0$ appear to give multi-pole strengths with magnitudes of order 1.

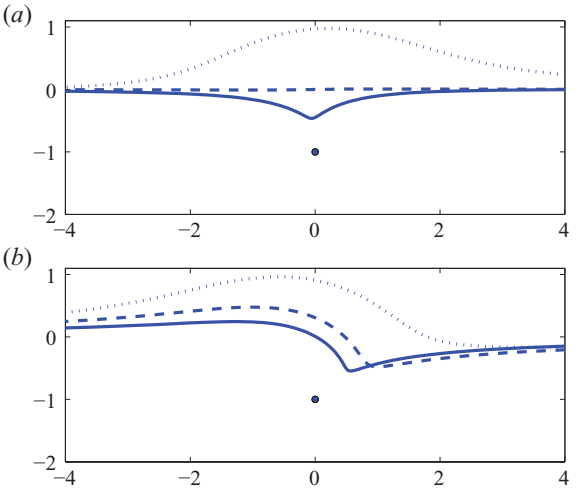

FIGURE 7. (Colour online) Free surface profiles with $Ca = 0.001$. (a) The solutions for $(a,c) = (1.54, 0.034)$ (solid), $(2, 0.008)$ (dashed) and $(2.96, 0.136)$ (dotted); (b) solutions for $(a,c) = (1.7, -0.366)$ (solid), $(2, -0.478)$ (dashed) and $(2.8, -0.396)$ (dotted).

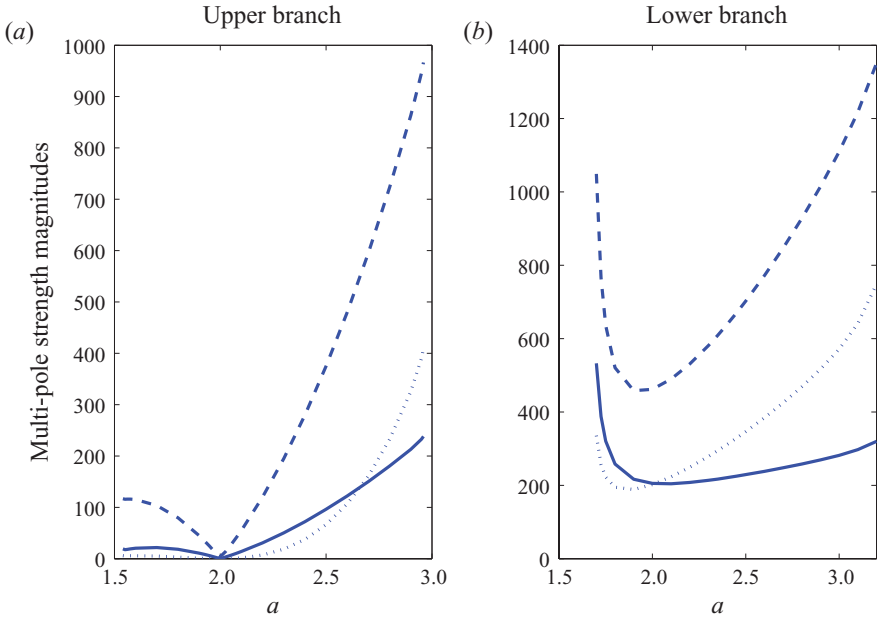

FIGURE 8. (Colour online) (a,b) Multi-pole strength magnitudes for $Ca = 0.001$: $|s^*|$ (solid), $|d^*|$ (dashed) and $|q^*|$ (dotted). Only the upper branch, with $a \approx 2$, yields multi-pole strengths of order 1 magnitude.

These solutions are close to the flat state. Figure 9 shows a close-up of the graphs of the multi-pole strength magnitudes near this close to flat state solution.

Interestingly, when $Ca = 0.001$ it is found that $|q^*| \to 0$ and $|d^*| \to 4$, which are the values obtained in § 4 for the flat state solution, cf. (5.47), by the method of images; but $|s^*|$ does *not* tend to the value 2 relevant to the flat state. This is to be expected because we have already determined in § 4 that there is no admissible

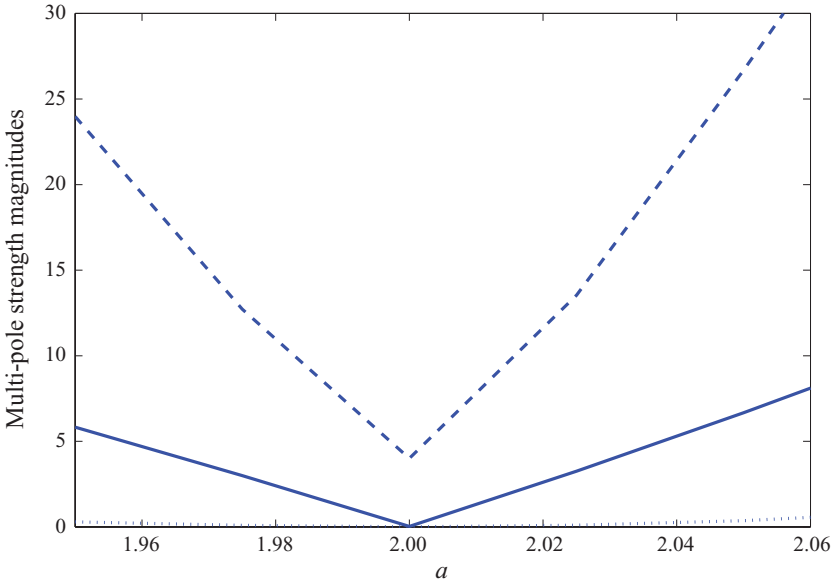

FIGURE 9. (Colour online) Close-up, near $a = 2$, of the graph in figure 8 of multi-pole strength magnitudes for the upper solution branch when $Ca = 0.001$: $|s^*|$ (solid), $|d^*|$ (dashed) and $|q^*|$ (dotted). The graph of $|q^*|$ is difficult to see – it is very close to the a-axis.

non-rotating solution when the surface is flat. For $a = 2$ we find that $c = 0.008$ with corresponding stresslet strength $|s^*| = 0.028$. This is evidence that even though the free-surface deformation is small, the surface tension is playing a key role here: while the free surface deformation is small, the fact that Ca^{-1} is large means that the contribution from the overall surface tension term still has an order 1 effect. Mathematically, surface tension appears to act as a singular perturbation to the system and appears to be essential for steady swimming.

Given that this is the most physically relevant régime, we now perform an asymptotic analysis of the full system for $Ca \ll 1$ near the flat state in order to properly understand the interplay of surface tension and surface deformability.

7. Asymptotic analysis for small *Ca*

The evidence so far suggests that, for small Ca, there exists a branch of steadily translating, non-rotating solutions in which the free surface is close to, but never quite attains, a flat state. Moreover, the associated multi-pole strengths in these solutions are of order unity. We now investigate this case in more detail by performing an asymptotic analysis of the full equations when $Ca \ll 1$ and when the interface is close to flat. For simplicity, we now fix $a = 2$, although the subsequent analysis can be repeated for arbitrary a close to 2. The conformal map then has the form

$$z(\zeta) = \frac{2}{\zeta + \mathrm{i}} + \mathrm{i} + \mathrm{i}c\zeta. \tag{7.1}$$

To proceed, we make the following asymptotic assumptions

$$0 < |c| \ll 1, \quad \frac{c}{Ca} = O(1). \tag{7.2}$$

Thus, we seek perturbations to the flat state that are small, and of the same order as the capillary number. It will be verified, *a posteriori*, by comparison with the exact solutions, that the assumed balance in (7.2) relating c and Ca is the relevant one as $Ca \to 0$. All expressions in the solution class can now be expanded in powers of c, with appropriate care taken because terms of the form c^2/Ca are $O(c)$, and not of $O(c^2)$ as they might appear at first sight. It is found from (5.25) that

$$I(\zeta, Ca) = \frac{1}{4Ca}\left[1 - \mathrm{i}\zeta + \frac{c}{4}(-5\zeta + 4\mathrm{i}\zeta^2 + \zeta^3) + \frac{\mathrm{i}c^2}{64}\left(-4\mathrm{i} + 36\zeta - 96\mathrm{i}\zeta^2 - 86\zeta^3 + 36\mathrm{i}\zeta^4 + 6\zeta^5\right)\right] + O(c^2). \tag{7.3}$$

This can be used in (5.24) to find an approximation to $F(\zeta)$ that is correct to $O(c)$. An approximation for $G(\zeta)$ follows from (5.31) with the observation that

$$\overline{z}(\zeta^{-1}) = z - \frac{\mathrm{i}c}{\zeta} - \mathrm{i}c\zeta. \tag{7.4}$$

These approximate expressions for $F(\zeta)$ and $G(\zeta)$ depend on C and D and, to find these, it is necessary to obtain approximations for the quantities f_0, f_1 and g_1. For this, it is helpful to make liberal use of the Laurent expansions,

$$\left.\begin{aligned} \zeta &= p_1(z+\mathrm{i}) + p_2(z+\mathrm{i})^2 + p_3(z+\mathrm{i})^3 + p_4(z+\mathrm{i})^4 + \cdots \\ \frac{1}{\zeta} &= \frac{\hat{p}_1}{(z+\mathrm{i})} + \hat{p}_2 + \hat{p}_3(z+\mathrm{i}) + \hat{p}_4(z+\mathrm{i})^2 + \cdots, \end{aligned}\right\} \tag{7.5}$$

where, before expansion in powers of c, exact expressions for the coefficients are

$$\left.\begin{aligned} p_1 &= \frac{1}{2+\mathrm{i}c}, \quad p_2 = -\frac{2\mathrm{i}}{(2+\mathrm{i}c)^3}, \quad p_3 = \frac{2}{(2+\mathrm{i}c)^4} - \frac{8}{(2+\mathrm{i}c)^5}, \\ p_4 &= \frac{2\mathrm{i}}{(2+\mathrm{i}c)^5} - \frac{20\mathrm{i}}{(2+\mathrm{i}c)^6} + \frac{40\mathrm{i}}{(2+\mathrm{i}c)^7}, \end{aligned}\right\} \tag{7.6}$$

with

$$\hat{p}_1 = \frac{1}{p_1}, \quad \hat{p}_2 = -\frac{p_2}{p_1^2}, \quad \hat{p}_3 = \frac{p_2^2}{p_1^3} - \frac{p_3}{p_1^2}, \quad \hat{p}_4 = -\frac{p_4}{p_1^2} + \frac{2p_2p_3}{p_1^3} - \frac{p_2^3}{p_1^4}. \tag{7.7}$$

All coefficients in (7.5) are expanded to $O(c^2)$; this is necessary, as just mentioned above, owing to the presence of terms in the equations proportional to $1/Ca$ which produce contributions of the order c^2/Ca which, under our assumptions, are $O(c)$. Armed with expressions for f_0, f_1 and g_1 (5.43)–(5.45) can be expanded correct to $O(c)$ and asymptotic solutions found for C and D. The algebra involved here is formidable, but it is helpful to have the solution to the full system available as an *a posteriori* check. Writing $C = C_x + \mathrm{i}C_y$ and $D = D_x + \mathrm{i}D_y$ it is found that

$$C_x = -\frac{1}{4} + \frac{c}{16Ca} + 4D_y, \quad C_y = \frac{1}{8Ca} - 2D_x + \frac{3c^2}{128Ca}, \tag{7.8}$$

with

$$D_x = \frac{3c^2}{32Ca} - \frac{13c}{8} + O(c^2), \quad D_y = \frac{1}{2} - \frac{c}{16Ca} + O(c^2). \tag{7.9}$$

Notice the appearance in these expressions both of terms proportional to c and terms proportional to c^2/Ca: this highlights the fact that the solutions result from a balance

between surface deformability (measured by c) and surface tension (measured by Ca). With C and D determined, $f(z)$ and $g(z)$ are known completely.

It still remains, however, to enforce the condition that the local vorticity at the swimmer location vanishes and this is expected to determine c as a function of Ca. This condition is found to require that

$$\mathrm{Im}[f_1] = -D_y - cD_x + O(c^2) = 0. \tag{7.10}$$

A combination of (7.9) and (7.10) then leads to the important relation

$$c = 8Ca. \tag{7.11}$$

This is consistent with the fact that it is the upper branch, with $c > 0$, that draws close to the flat state as $Ca \to 0$. It is also consistent with the parameter values $(a, c) = (2, 0.008)$ for the near-flat solution with $Ca = 0.001$ shown in figure 7. The asymptotic result (7.11) has been superposed on the graph in figure 6 and gives excellent agreement for small Ca, thereby validating our initial assumptions. From (7.9), we then find, for example, that

$$D_x = -7Ca + O(c^2), \quad D_y = O(c^2), \tag{7.12}$$

with similar expressions for C_x and C_y then available from (7.5). With C and D known, expressions for the strengths of the stresslet, dipole and quadrupole are found to be

$$s^* = -28Ca + O(Ca^2), \quad d^* = -4 - 80\mathrm{i}Ca + O(Ca^2), \quad q^* = O(Ca^2). \tag{7.13}$$

For the case $Ca = 0.001$, this gives

$$s^* = -0.028, \quad d^* = -4 - 0.08\mathrm{i}, \quad q^* = 0, \tag{7.14}$$

which is consistent with the results reported in § 6 based on evaluation of the full solutions.

In summary, by an asymptotic analysis of the exact solutions, it has been demonstrated explicitly that surface tension serves to provide a mechanism for steady swimming. When the capillary number Ca is small, solutions for steady, non-rotating swimmers are possible with free surface deflections of the same order as Ca, with multi-pole strengths scaling as in (7.13). Both surface tension and interface deformability are crucial for the mechanism since it results from a balance between terms of $O(c)$ and terms of $O(c^2/Ca)$.

8. Conclusion

In this paper, we have used a two-dimensional model, amenable to the methods of complex analysis, to identify a new mode of low-Reynolds number swimming, namely organisms or devices that exploit the deformation of a nearby free capillary surface in order to swim steadily along it. All swimmers are taken to translate at unit speed in the horizontal direction beneath the free surface and, for a chosen Ca, we find the associated free surface shape and multi-pole strengths. For physically realistic values of $Ca \ll 1$, we identify the possibility of steady, non-rotating locomotion for weakly deformed interfaces close to the flat state. The slight deformation of the interface from flat, and the non-zero surface tension, are crucial for the mechanism. For larger capillary numbers, steady locomotion is also possible provided the free surface deformation from the flat state is sufficiently large.

The bearing of our two-dimensional analysis on the physics of actual organisms employing a free surface for propulsion is not yet clear but we believe that it has unveiled a fundamental physical mechanism. The essence of this mechanism will likely also pertain to fully three-dimensional swimmers. Other models for free surface locomotion have been proposed taking into account the lubrication forces between the swimmer and the free surface (Lee et al. 2008). Other important physical effects, not considered in this study, could include the presence of a layer of viscoelastic mucus between the foot of a water snail and the free surface. Such effects may play an important role and have not been considered in this study, although we have successfully unveiled a basic mechanism for the steady locomotion of a swimmer near a free capillary surface without the need to incorporate any additional physical effects and demonstrated the essential role played by interface deformability.

The point swimmer model we have used is motivated by a simple treadmilling circular motion of the kind first considered by Blake (1971*b*) and, in light of our analysis, it is worth referring back to these earlier motivations. Crowdy & Or (2010) considered circular surface treadmilling swimmers with an imposed tangential surface velocity of the special form,

$$U(\phi, t) = 2V \sin(2(\phi - \theta(t))), \tag{8.1}$$

and found that such a swimmer has an effective point singularity description consisting of a stresslet of strength $\mu(t) = \epsilon V \exp(2\mathrm{i}\theta(t))$ with a superposed potential quadrupole of strength $2\mu(t)\epsilon^2$. If, instead, we considered a circular treadmilling swimmer with a tangential surface velocity of the generalized form

$$U(\phi, t) = 2W \sin(\phi - \theta(t)) + 2V \sin(2(\phi - \theta(t))), \tag{8.2}$$

where W and V are parameters then the equivalent singularity description can similarly be shown to comprise a stresslet together with a superposed potential quadrupole *and* dipole contribution; the strengths of these multi-poles are linearly related to the values of the imposed surface velocity parameters W and V. Thus, the effective point singularity description of this generalized treadmilling swimmer is of precisely the kind considered in this paper. Our results therefore suggest the possibility of carrying out a formal asymptotic matching procedure where a small, finite-area circular treadmiller, with an imposed profile of the form (8.2), is 'matched' to an outer flow described using an analytical solution akin to that presented here. The relevant inner–outer matching conditions will involve ensuring that the far-field multi-poles generated by the particular choices of W and V for the local swimmer model match the values of s^*, d^* and q^* needed for steady swimming in the far-field. Full details of such an analysis are reserved for a future investigation. Antanovskii (1996) has used precisely such a strategy of matched asymptotics in his two-dimensional complex variable model of a deformable bubble in the flow field generated by Taylor's four-roller mill.

It is likely that, as in the case of swimming near a no-slip wall, the generic locomotion mechanism of an organism near a free surface will have a more complicated spatio-temporal structure. Indeed, free surface deflection associated with unsteady undulatory waves propagating along the foot of a water snail have been observed in practice. In future work, it may be interesting to study the full unsteady dynamics of a point swimmer near a free capillary surface. The geometrical complexities even in that simplified case would no doubt require a fully numerical investigation. Without considerably more work we are unable to say anything here

about the stability of the steady solutions although this is clearly of interest. This is left as a topic for future study.

This work was funded in part by the US National Science Foundation through grants CTS-0624830 (EL and AEH) and CBET-0746285 (EL). D.C. acknowledges the support of an EPSRC Advanced Research Fellowship as well as the hospitality of the Department of Mathematics at MIT where this work was initiated. O.S. also acknowledges support from an EPSRC studentship.

REFERENCES

Ablowitz, M. & Fokas, A. S. 1997 *Complex Variables*. Cambridge University Press.

Antanovskii, L. I. 1996 Formation of a pointed drop in Taylor's four-roller mill. *J. Fluid Mech.* **327**, 325.

Batchelor, G. K. 1970 The stress system in a suspension of force-free particles. *J. Fluid Mech.* **41**, 545–570.

Berg, H. C. & Turner, L. 1990 Chemotaxis of bacteria in glass capillary arrays - *Escherichia coli,* motility, microchannel plate, and light scattering. *Biophys. J.* **58**, 919–930.

Berke, A. P., Turner, L., Berg, H. C. & Lauga, E. 2008 Hydrodynamic attraction of swimming microorganisms by surfaces. *Phys. Rev. Lett.* **101**, 038102.

Blake, J. R. 1971*a* A note on the image system for a Stokeslet in a no-slip boundary. *Proc. Camb. Phil. Soc.* **70**, 303–310.

Blake, J. R. 1971*b* Self propulsion due to oscillations on the surface of a cylinder at low Reynolds number. *Bull. Austral. Math. Soc.* **5**, 255–264.

Blake, J. R. & Chwang, A. T. 1974 Fundamental singularities of viscous-flow. Part 1. Image systems in vicinity of a stationary no-slip boundary. *J. Engng Maths* **8**, 23–29.

Brennen, C. & Winet, H. 1977 Fluid mechanics of propulsion by cilia and flagella. *Annu. Rev. Fluid Mech.* **9**, 339.

Clift, A. F. & Hart, J. 1953 Variations in the apparent viscosity of human cervical mucus. *J. Physiol.* **122** (2), 358–365.

Copeland, M. 1919 Locomotion in two species of the gastropod genus alectrion with observations on the behavior of pedal cilia. *Biol. Bull.* **37**, 126–138.

Copeland, M. 1922 Ciliary and muscular locomotion in the gastropod genus polinices. *Biol. Bull.* **42**, 132–142.

Cosson, J., Huitorel, P. & Gagnon, C. 2003 How spermatozoa come to be confined to surfaces. *Cell Motil. Cytoskel.* **54**, 56–63.

Costerton, J. W., Lewandowski, Z., Caldwell, D. E., Korber, D. R. & Lappinscott, H. M. 1995 Microbial biofilms. *Ann. Rev. Microbiol.* **49**, 711–745.

Crowdy, D. G. 2011 Treadmilling swimmers near a no-slip wall at low Reynolds number. *Intl J. Non-Linear Mech.* **46**, 577–585.

Crowdy, D. G. & Or, Y. 2010 Two-dimensional point singularity model of a low Reynolds number swimmer near a wall. *Phys. Rev.* E **81**, 036313.

Fauci, L. J. & Mcdonald, A. 1995 Sperm motility in the presence of boundaries. *Bull. Math. Biol.* **57**, 679–699.

Frymier, P. D. & Ford, R. M. 1997 Analysis of bacterial swimming speed approaching a solid–liquid interface. *AlChE J.* **43**, 1341–1347.

Hatwalne, Y., Ramaswamy, S., Rao, M. & A., Simha R. 2004 Rheology of active-particle suspensions. *Phys. Rev. Lett.* **92**, 118101.

Hernandez-Ortiz, J. P., Stoltz, C. G. & Graham, M. D. 2005 Transport and collective dynamics in suspensions of confined swimming particles. *Phys. Rev. Lett.* **95**, 204501.

Jeong, J. 1999 Formation of cusp on the free surface at low Reynolds number flow. *Phys. Fluids* **11**, 521–526.

Jeong, J. & Moffatt, H. K. 1992 Free-surface cusps associated with flow at low Reynolds number. *J. Fluid Mech.* **241**, 1–22.

Katz, D. F. & Blake, J. R. 1975 Flagellar motions near walls. In *Swimming and Flying in Nature* (ed. T. Y. Wu, C. J. Brokaw & C Brennen), vol. 1, pp. 173–184. Plenum.

Katz, D. F. 1974 Propulsion of microorganisms near solid boundaries. *J. Fluid Mech.* **64**, 33–49.

Katz, D. F., Blake, J. R. & Paverifontana, S. L. 1975 Movement of slender bodies near plane boundaries at low Reynolds number. *J. Fluid Mech.* **72**, 529–540.

Langlois, W. E. 1964 *Slow Viscous Flow*. Macmillan.

Lauga, E., DiLuzio, W. R., Whitesides, G. M. & Stone, H. A. 2006 Swimming in circles: Motion of bacteria near solid boundaries. *Biophys. J.* **90**, 400–412.

Lauga, E. & Powers, T. R. 2009 The hydrodynamics of swimming microorganisms. *Rep. Prog. Phys.* **72**, 096601.

Lee, S., Bush, J. W. M., Hosoi, A. E. & Lauga, E. 2008 Crawling beneath the free surface: Water snail locomotion. *Phys. Fluids* **20**, 082106.

Maeda, K., Imae, Y., Shioi, J. I. & Oosawa, F. 1976 Effect of temperature on motility and chemotaxis of *Escherichia coli*. *J. Bacteriol.* **127**, 1039–1046.

Or, Y. & Murray, R. 2009 Dynamics and stability of a class of low Reynolds number swimmers near a wall. *Phys. Rev.* E **79**, 045302.

Pedley, T. J. & Kessler, J. O. 1992 Hydrodynamic phenomena in suspensions of swimming microorganisms. *Annu. Rev. Fluid Mech.* **24**, 313–358.

Pozrikidis, C. 1992 *Boundary Integral and Singurality Methods for Linearized Viscous Flow*. Cambridge University Press.

Reynolds, A. J. 1965 The swimming of minute organisms. *J. Fluid Mech.* **23**, 241–260.

Rothschild, L. 1963 Non-random distribution of bull spermatozoa in a drop of sperm suspension. *Nature* **198**, 1221.

Suarez, S. S. & Pacey, A. A. 2006 Sperm transport in the female reproductive tract. *Human Reprod. Update* **12**(1), 23–37.

Trouilloud, R., Yu, T. S., Hosoi, A. E. & Lauga, E. 2008 Soft swimming: Exploiting deformable interfaces for low Reynolds number locomotion. *Phys. Rev. Lett.* **101**, 048102.

Urzay, J. 2010 Asymptotic theory of the elastohydrodynamic adhesion and gliding motion of a solid particle over soft and sticky substrates at low Reynolds numbers. *J. Fluid Mech.* **653**, 391–429.

Winet, H., Bernstein, G. S. & Head, J. 1984 Observations on the response of human spermatozoa to gravity, boundaries and fluid shear. *J. Reprod. Fertil.* **70**, 511–523.

Woolley, D. M. 2003 Motility of spermatozoa at surfaces. *Reproduction* **126**, 259–270.

Zhang, S., Or, Y. & Murray, R. 2010 Experimental demonstration of the dynamics and stability of a low Reynolds number swimmer near a plane wall. In *Proc. American Control Conference (ACC)*, pp. 4205–4210.